Stability Sensitivity Analysis of a Helicopter Rotor

Joon W. Lim* and Inderjit Chopra†
University of Maryland, College Park, Maryland

A sensitivity study of blade stability in forward flight for a hingeless rotor with respect to design variables is carried out using a direct analytical method. Design variables include nonstructural mass distribution (spanwise and chordwise), chordwise offset of center of gravity, and blade bending stiffnesses (flap, lag, and torsion). The formulation for blade steady response is based on a finite-element method in space and time. The vehicle trim and blade steady response are calculated iteratively as one coupled solution using a modified Newton method (coupled trim analysis). Eigenvalues corresponding to different blade modes are calculated using Floquet transition matrix theory. The formulation for the derivatives of the eigenvalues with respect to the design variables is implemented using a direct analytical approach and constitutes an integral part of the regular stability analysis. For the calculation of the stability derivatives with respect to a total of 30 design variables, there is an 85% reduction in CPU time using the direct analytical approach compared to the frequently adopted finite-difference approach. A parametric study showed that nonstructural mass and chordwise blade c.g. offset of outboard elements, and lag bending stiffness of inboard elements, have powerful influence on blade stability.

Nomenclature

$\boldsymbol{B}$ = characteristic exponent
$\boldsymbol{C}$ = global perturbation damping matrix
c = blade chord
c_d, c_l, c_m = blade section drag, lift, and moment coefficients, respectively
$\boldsymbol{D}$ = design variables; D_j, $j = 1,\ldots,n$
EI_y, EI_z = blade flap and lag, respectively, bending stiffness
e_A, e_d = chordwise offset of tensile axis and aerodynamic center, respectively, from the elastic axis (positive forward)
$\boldsymbol{f}$ = vehicle equilibrium equations
GJ = blade torsional stiffness
$\boldsymbol{K,M}$ = global perturbation stiffness and mass matrices, respectively
$\boldsymbol{k,m}$ = normalized perturbation stiffness and mass matrices, respectively
m_0, m_{ns} = baseline and nonstructural mass per unit length
n = number of design variables
$\boldsymbol{p}$ = normal mode coordinates
$\boldsymbol{q}$ = blade global coordinates
T = time period of one rotor revolution, 2π rad
$\boldsymbol{V_t}$ = vehicle trim parameters
$\boldsymbol{X}$ = state variables of normal mode coordinates
y_0, y_{ns} = chordwise offset of baseline blade c.g. and nonstructural mass, respectively, from the elastic axis (positive forward)
α_k = real part of eigenvalue of the kth mode
α_s = longitudinal tilt of shaft (positive forward)
ψ = azimuth angle, Ωt
σ = solidity ratio, $N_b c/\pi R$
Φ = transition matrix of perturbation equations
Φ = modal matrix
ϕ_s = lateral tilt of shaft (positive advancing side down)
$\theta_{.75}$ = collective pitch angle at 75% blade span
θ_{1c}, θ_{1s} = longitudinal and lateral cyclic pitch angles, respectively.
λ_k = eigenvalue of the kth mode
ω_k = imaginary part of eigenvalue of the kth mode
μ = advance ratio

Introduction

WITH an enhanced understanding of the dynamics of rotary-wing systems, it is now becoming feasible to apply modern structural optimization techniques to reduce vibration, hub loads, and structural bending and to improve performance and aeroelastic stability margins. The potential of aeroelastic optimization is further expanded with the application of advanced composites, which permit great flexibility in tailoring structural characteristics. Recently, some selected attempts have been made to apply aeroelastic optimization to the rotary-wing field.[1-9] In spite of numerous restrictions and assumptions embedded in these investigations, these papers showed the potential of aeroelastic optimization to rotor systems.

Aeroelastic optimization of the system consists essentially of calculating the optimum values of the design variables that minimize the objective function and satisfy certain aeroelastic and geometric constraints. One of the key elements of an optimization study is the design sensitivity analysis. This involves calculation of the sensitivity derivatives of the objective function, such as hub loads, structural bending, and blade response and of aeroelastic constraints, such as eigenvalues. Rotor dynamics is complex and involves nonlinear inertial, elastic and aerodynamic forces. Therefore, it is important to carry out the sensitivity analysis as efficiently as possible for the rotor optimization problems. Adelman and Haftka[10] have given a general survey paper on the sensitivity analysis of a discrete structural system, where the importance of the calculation of design sensitivity derivatives in structural optimization problems is stressed. Existing rotor optimization studies use finite-difference methods to calculate gradients and therefore require a substantial computational effort to obtain an optimum solution. Because of prohibitively large computation time, most of the studies are restrictive in terms of objective

Presented as Paper 88-2310 at the AIAA/ASME/ASCE/AHS 29th Structures, Structural Dynamics, and Materials Conference, Williamsburg, VA, April 18-20, 1988; received Sept. 23, 1988; revision received May 8, 1989.

*Research Associate; currently at Bell Helicopter Textron, Ft. Worth, TX.

†Professor of Department of Aerospace Engineering. Associate Fellow AIAA.

functions, dynamic constraints, and number of design variables. Recently, Celi and Friedmann[9] addressed this issue by building a sequence of approximate optimization problems. This method reduced the total number of function evaluations in the optimization process. In Ref. 11, the authors have also addressed this issue by developing a computationally efficient procedure to calculate gradient information of blade response and hub loads with respect to structural design parameters. This procedure was formulated by coupling a direct analytical approach with a finite-element method in time. The sensitivity derivatives of steady response and hub loads constitute an integral part of the basic trim and response calculations, and these were calculated at a fraction of the computation time required in the frequently adopted finite-difference approach.

The present paper formulates the stability sensitivity analysis of a helicopter rotor blade in forward flight for an aeroelastic optimization. A systematic parametric study is carried out by redistributing structural and inertial characteristics of the blade. Design variables include spanwise and chordwise distribution of a nonstructural mass, chordwise offset of blade center of gravity, and blade bending stiffnesses (flap, lag, and torsion). Using a direct analytical approach, derivatives of eigenvalues corresponding to different blade modes with respect to design variables are derived from Floquet transition matrix theory and constitute an integral part of the regular stability analysis.

For effective stability sensitivity analysis, one needs a reliable analysis procedure to determine steady response and stability of a rotor system in forward flight. Over the years, there have been several contributions to the development of a reliable procedure for rotor dynamics analysis.[12,13] The coupled rotor dynamics analysis used in the present study is a comprehensive code developed at the University of Maryland and is based on a finite-element method in space and time.[14,15] This analysis consists of two major phases: vehicle trim and rotor steady response (coupled trim analysis) and aeroelastic stability of the blade. The vehicle trim solution determines the control settings and vehicle attitude for the prescribed flight condition. The trim is characterized in terms of five rigid-body nonlinear forces and moments equilibrium equations, which are coupled with rotor equations. The steady response involves the determination of time-dependent blade deflections at different azimuth positions for the time period of one complete cycle using finite-element method in time. The vehicle trim and blade steady response are calculated iteratively as one coupled solution using a modified Newton method. For the aeroelastic stability solution, the linearized blade perturbation equations are transformed to the normal mode space, and then blade damping is calculated using Floquet transition matrix theory.

Analysis

The rotor dynamics analysis is based on a finite-element method in space and time. Each blade is assumed to be an elastic beam undergoing flap bending, lag bending, elastic twist, and axial deflections. The blade is discretized into a number of beam elements. Each beam element consists of 15 degrees of freedom. Between elements, there is a continuity of displacement and slope for lag and flap bending deflections and a continuity of displacement for elastic twist and axial deflections. The analysis is developed for a nonuniform blade having pretwist, precone, and chordwise offsets of blade center of gravity (c.g.), aerodynamic center, and tensile axis from the elastic axis.

Aerodynamic loads are obtained based on a quasisteady strip theory approximation. The noncirculatory loads based on unsteady thin airfoil theory are also included. For the steady induced inflow distribution on the rotor disk, the Drees linear inflow model[16] is used.

The analysis involves calculation of trim, and then calculation of blade damping. From the coupled trim analysis, control settings, vehicle attitude, blade steady response and hub loads are determined. Then, using Floquet transition matrix theory, rotor blade damping and its sensitivity derivatives are obtained.

Coupled Trim Analysis

Coupled trim analysis in forward flight consists of vehicle trim (propulsive), blade steady response, and hub loads calculation. The trim solution is calculated from the overall nonlinear vehicle equilibrium equations: three force equations (vertical, longitudinal, and lateral) and two moments equations (pitch and roll). The yawing moment equilibrium equation is not included since the yawing angle is considered to have small influence on rotor response and stability solutions. For a specified advance ratio μ and weight coefficient c_W, the propulsive trim solution determines pilot-control settings ($\theta_{.75}$, θ_{1c}, θ_{1s}) and vehicle attitude (α_s, ϕ_s).

The blade steady response solution involves the determination of time-dependent blade deflections at different azimuth locations. This steady response solution is calculated using a finite-element method in time, which is formulated from Hamilton's weak principle. The blade steady response equations are nonlinear periodic equations. For the response solution, the time period of one rotor revolution is discretized into a number of time elements, and then the periodicity of response is imposed on the assembling of finite-element equations. To reduce computation time, these equations are transformed to the normal mode domain using the coupled natural vibration modes of the blade. Then, the steady response is calculated from the nonlinear algebraic normal mode equations.

The hub loads are then obtained using a force summation method. For this, motion-induced aerodynamic and inertial loads are integrated along the blade span to obtain blade loads at the root, and then summed over all the blades to obtain the rotor hub loads.

The vehicle equilibrium equations show inherent couplings between a rotor and fuselage of a helicopter. For a coupled trim solution, the propulsive trim solution based on rigid flap rotor dynamics is used as an initial guess at first iteration and, in the subsequent iterations, vehicle trim and rotor response are calculated as one coupled solution using a modified Newton method. It is noted that the overall vehicle forces and moments equilibrium equations are always satisfied by a converged coupled trim solution.

For the coupled trim analysis, the nonlinear vehicle equilibrium equations can be linearized about the vehicle parameters using a Taylor series expansion such as

$$f(V_t + \Delta V_t) = f(V_t) + \frac{\partial f}{\partial V_t} \cdot \Delta V_t = 0 \tag{1}$$

where vehicle trim parameters V_t are defined as α_s, ϕ_s, $\theta_{.75}$, θ_{1c}, and θ_{1s}, and f implies the vehicle equilibrium equations (refer to Refs. 17 and 18). The increment of the vehicle trim parameters is given from the preceding equations in the following form:

$$\Delta V_t = -\left(\frac{\partial f}{\partial V_t}\right)^{-1} f(V_t) \tag{2}$$

Table 1 Baseline hingeless blade structural properties

$EI_y/m_0\Omega^2R^4$	0.01080
$EI_z/m_0\Omega^2R^4$	0.02680 (soft)
	0.14400 (stiff)
$GJ/m_0\Omega^2R^4$	0.00615
k_A/R	0.0290
k_{m1}/R	0.0132
k_{m2}/R	0.0247

The $\partial f/\partial V_t$ is a Jacobian (tangential) matrix. This Jacobian matrix is calculated by a forward finite-difference approach. To reduce computation time, a modified Newton method is adopted. Hence, the Jacobian matrix is saved in the first iteration step. The vehicle trim parameters V_t can be calculated iteratively using

$$V_t^{(n)} = V_t^{(n-1)} + \Delta V_t^{(n)} \tag{3}$$

where n is the step of iteration. For a converged solution, $\Delta V_t^{(n)}$ becomes nearly zero. In the coupled trim analysis, the blade steady response X_G, as well as the vehicle trim parameters V_t, must be converged at the same time. For a completely converged solution, the following must therefore be satisfied:

$$\begin{Bmatrix} \Delta X_G^{(n)} \\ \Delta V_t^{(n)} \end{Bmatrix} \to 0 \tag{4}$$

Blade Perturbation Equations of Motion

The perturbation equations of motion are obtained by linearizing the blade equations about the blade's steady deflected position. The resulting perturbation equations can be written concisely as

$$M\delta\ddot{q} + C\delta\dot{q} + K\delta q = 0 \tag{5}$$

where M, C, and K are the global finite-element perturbation matrices. To reduce computation time, these equations are transformed into the normal mode domain using the coupled free-vibration characteristics of the blade about the mean deflected position. For this, the displacement vector can be written as

$$q = \Phi p \tag{6}$$

where the matrix Φ contains m columns, each respectively representing a particular mode. Substituting this displacement into perturbation equations, one would obtain the following normal mode equations:

$$m\delta\ddot{p} + c\delta\dot{p} + k\delta p = 0 \tag{7}$$

where

$$m = \Phi^T M \Phi$$
$$c = \Phi^T C \Phi$$
$$k = \Phi^T K \Phi$$

The normalized perturbation matrices contain periodic coefficients and also are not diagonal since these contain motion-dependent aerodynamic forces. For the stability analysis, the preceding equations are transformed to the first-order form:

$$\delta\dot{X} = A(\psi)\delta X \tag{8}$$

where

$$\delta X = \begin{Bmatrix} \delta p \\ \delta\dot{p} \end{Bmatrix}$$
$$A(\psi) = \begin{bmatrix} 0 & I \\ -m^{-1}k & -m^{-1}c \end{bmatrix}$$

These are $2m$ linear equations, where m is the number of normal modes.

Aeroelastic Stability Analysis

The aeroelastic stability of the rotor in forward flight is formulated using Floquet transition matrix theory. Let us consider the blade perturbation equations in the first-order form with periodic coefficients. By definition, the state transition matrix Φ, which is sometimes called the fundamental matrix, must satisfy these linear differential equations with the initial conditions of an identity matrix,

$$\dot{\Phi}(\psi,\psi_0) = A(\psi)\Phi(\psi,\psi_0) \tag{9}$$

The transition matrix has the following properties[19]:

Property 1 (definition):

$$\Phi(\psi_0,\psi_0) = I \tag{10}$$

Property 2 (path independence):

$$\Phi(\psi_2,\psi_0) = \Phi(\psi_2,\psi_1)\Phi(\psi_1,\psi_0) \tag{11}$$

Property 3:

$$\Phi(\psi_1,\psi_0) = \Phi^{-1}(\psi_0,\psi_1) \tag{12}$$

The matrix A is a continuous periodic matrix with a period of T, such as

$$A(\psi) = A(\psi + T) \tag{13}$$

If $\Phi(\psi,\psi_0)$ is a state transition matrix for linear differential equations, then a constant nonsingular matrix B exists such that

$$\Phi(\psi + T,\psi_0) = \Phi(\psi,\psi_0)e^{BT} \tag{14}$$

Note e^{BT} is called the characteristic multiplier and the matrix B is referred to as the characteristic exponent. Using Eq. (9), this relationship can be easily proved as follows:

$$\begin{aligned}\dot{\Phi}(\psi + T,\psi_0) &= \dot{\Phi}(\psi,\psi_0)e^{BT} \\ &= A(\psi)\Phi(\psi,\psi_0)e^{BT} \\ &= A(\psi)\Phi(\psi + T,\psi_0)\end{aligned}$$

and this shows that $\Phi(\psi + T,\psi_0)$ also satisfies the linear differential equations. The characteristic multiplier e^{BT} can be a measure of stability since the growth or decay of the transition matrix depends on the properties of the characteristic multiplier [Eq. (14)]. Note that, in general, the characteristic exponent cannot be determined uniquely since it is one of the multiple solutions of the complex logarithm of the characteristic multiplier, but this characteristic exponent will be invariant under a similarity transformation.

For the stability, the eigenvalue equation of the characteristic multiplier is put in the following form:

$$e^{BT}x = \lambda x \tag{15}$$

Choosing $\psi = \psi_0$ in Eq. (14) gives

$$e^{BT} = \Phi(\psi_0 + T,\psi_0) \tag{16}$$

This relation implies that the characteristic multiplier is equivalent to the value of the transition matrix at the end of one time period, regardless of initial time ψ_0. Therefore, by examining the eigenvalues of the $\Phi(\psi_0 + T,\psi_0)$, the blade stability can be determined. Using Eq. (16), the eigenvalue equation can therefore be rewritten in terms of the transition matrix, such that

$$\Phi(\psi_0 + T,\psi_0)x = \lambda x \tag{17}$$

where the x is generally the complex eigenvector. To solve this eigenvalue equation, one needs to calculate the transition matrix $\Phi(\psi_0 + T,\psi_0)$, which has a size of $2m \times 2m$ if m normal modes are used in the analysis. From Eq. (9), the transition

matrix can be calculated using any linear differential equations solver, such as the Runge-Kutta, Adams-Bashforth, and Adams predictor-corrector methods. In the present analysis, the Adams predictor-corrector method with variable step size is used.

Once $\Phi(\psi_0 + T, \psi_0)$ is calculated, the eigenvalue equation (17) can be solved using any standard complex eigensystem solver. The complex eigenvalue λ_k of the kth mode can be written as

$$\lambda_k = \lambda_k^R + i\lambda_k^I = \exp[(\alpha_k + i\omega_k)T] \tag{18}$$

where the superscripts R and I denote the real and imaginary parts of the eigenvalue. The α_k and frequency ω_k of the kth mode are defined such that

$$\alpha_k = \frac{1}{T} \ell n \sqrt{(\lambda_k^R)^2 + (\lambda_k^I)^2}$$

$$\omega_k = \frac{1}{T} \tan^{-1}\left(\frac{\lambda_k^I}{\lambda_k^R}\right) \tag{19}$$

It may be noted that blade damping is defined by α_k with a negative sign. The α_k measures the growth or decay of the kth mode response. If α_k is positive, the mode is unstable. If α_k is negative, the mode is stable. If α_k is zero, the mode is neutral. The ω_k represents the frequency of vibration. Since the inverse tangent function is multivalued, one will get multivalues of ω_k. Using constant coefficient approximations,[17] the proper value for ω_k is selected.

Stability Sensitivity Analysis

For stability sensitivity derivatives, a direct analytical approach[10,11] is employed. Let us consider a general function F, which depends on design variables $\boldsymbol{D}$ and blade response $\boldsymbol{Y}$, such as

$$F = F(\boldsymbol{D}, \boldsymbol{Y}(\boldsymbol{D})) \tag{20}$$

The sensitivity derivatives of this function are calculated as

$$\frac{dF}{dD_j} = \frac{\partial F}{\partial D_j} + \frac{\partial F}{\partial Y}\frac{\partial Y}{\partial D_j}, \qquad j = 1,\ldots, n \tag{21}$$

The function F can be any of the blade loads, hub loads, or eigenvalues

For the sensitivity derivatives, a finite-difference approach is more commonly adopted. The finite-difference approach is easy to implement but requires considerable computation time. Also, the selection of proper step size is often not easy. The analytical approach requires explicit expressions but reduces the computation time substantially. This analytical approach appears to have great potential for complex rotorcraft optimization problems. In the present study, both approaches are implemented.

The stability sensitivity derivatives are obtained using Floquet transition matrix theory. By simply differentiating Eq. (9) with respect to design variables, linear differential equations for the derivatives of the transition matrix are given in the following form:

$$\frac{d\dot{\Phi}}{dD_j} = A\frac{d\Phi}{dD_j} + \frac{dA}{dD_j}\Phi, \qquad j = 1,\ldots, n \tag{22}$$

Differentiating the path independence property of the transition matrix [Eq. (11)] with respect to design variables, one would obtain the following equation:

$$\frac{d\Phi(\psi_2,\psi_0)}{dD_j} = \Phi(\psi_2,\psi_1)\frac{d\Phi(\psi_1,\psi_0)}{dD_j} + \frac{d\Phi(\psi_2,\psi_1)}{dD_j}\Phi(\psi_1,\psi_0) \tag{23}$$

Letting $\psi_1 = \psi_0$ and using the definition of the transition matrix in Eq. (10), the initial conditions for the derivatives of the transition matrix are derived as

$$\frac{d\Phi(\psi_0,\psi_0)}{dD_j} = 0, \qquad j = 1,\ldots, n \tag{24}$$

Rewriting the linear differential equations for the derivatives of the transition matrix, one would obtain

$$\frac{d}{d\psi}\begin{Bmatrix} \Phi \\ \frac{d\Phi}{dD_1} \\ \frac{d\Phi}{dD_2} \\ \vdots \\ \frac{d\Phi}{dD_n} \end{Bmatrix} = \begin{bmatrix} A & 0 & 0 & \cdots & 0 \\ \frac{dA}{dD_1} & A & 0 & \cdots & 0 \\ \frac{dA}{dD_2} & 0 & A & \ddots & \vdots \\ \vdots & \vdots & \ddots & \ddots & 0 \\ \frac{dA}{dD_n} & 0 & \cdots & 0 & A \end{bmatrix} \begin{Bmatrix} \Phi \\ \frac{d\Phi}{dD_1} \\ \frac{d\Phi}{dD_2} \\ \vdots \\ \frac{d\Phi}{dD_n} \end{Bmatrix} \tag{25}$$

and the initial conditions are

$$\begin{Bmatrix} \Phi \\ \frac{d\Phi}{dD_1} \\ \vdots \\ \frac{d\Phi}{dD_n} \end{Bmatrix} = \begin{Bmatrix} I \\ 0 \\ \vdots \\ 0 \end{Bmatrix} \quad \text{at } \psi = \psi_0 \tag{26}$$

Note that differential operators $d/d\psi$ and d/dD_j are interchangeable. The transition matrix and its derivatives with respect to design variables can be calculated for any ψ from the preceding linear differential equations using the Adams predictor-corrector method.

The eigenvalue equation in Eq. (17) is associated with the transition matrix. The derivatives of eigenvalues can be expressed in terms of the transition matrix. By differentiating the eigenvalue equation with respect to design variables, the following relation is obtained:

$$\frac{d\lambda_k}{dD_j}\boldsymbol{x}_k = \frac{d\Phi}{dD_j}\boldsymbol{x}_k + (\Phi - \lambda_k I)\frac{d\boldsymbol{x}_k}{dD_j} \tag{27}$$

It is noted that the second term in the righthand side is dropped out due to Eq. (17). Premultiplying both sides of Eq. (27) by $\boldsymbol{y}_k^T$, where the $\boldsymbol{y}_k$ is the left eignevector of Eq. (17) and satisfies

$$\boldsymbol{y}_k^T\Phi = \lambda_k\boldsymbol{y}_k^T \tag{28}$$

one would obtain the derivatives of the kth eigenvalue as follows:

$$\frac{d\lambda_k}{dD_j} = \frac{d\lambda_k^R}{dD_j} + i\frac{d\lambda_k^I}{dD_j} = \boldsymbol{y}_k^T\frac{d\Phi(\psi_0 + T, \psi_0)}{dD_j}\boldsymbol{x}_k \tag{29}$$

where

$$\boldsymbol{y}_k^T\boldsymbol{x}_k = 1 \tag{30}$$

After the eigenvalue derivatives are calculated, the stability derivatives can be obtained by simply differentiating α_k with respect to design variables. Therefore, by differentiating Eq. (19), the derivatives of α_k are given as

$$\frac{d\alpha_k}{dD_j} = \frac{1}{T}\frac{\lambda_k^R\frac{d\lambda_k^R}{dD_j} + \lambda_k^I\frac{d\lambda_k^I}{dD_j}}{(\lambda_j^R)^2 + (\lambda_k^I)^2} \tag{31}$$

where the period T is chosen as 2π.

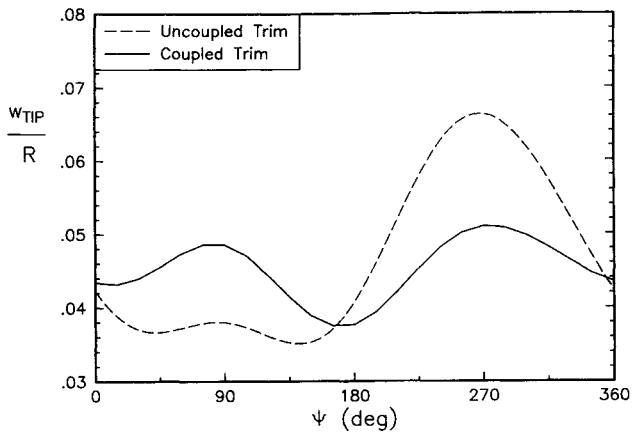

Fig. 1 Steady flap response at tip.

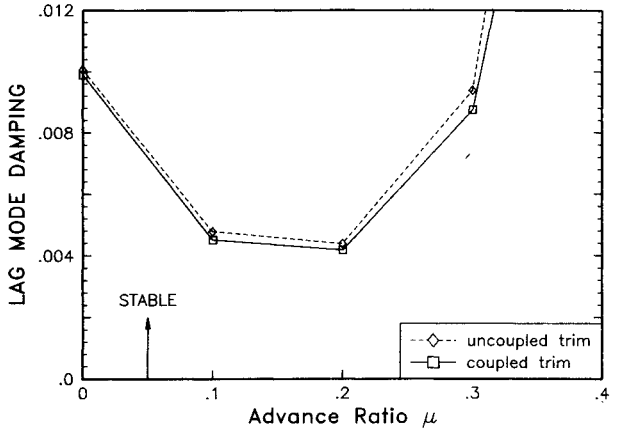

Fig. 2a Fundamental lag mode damping.

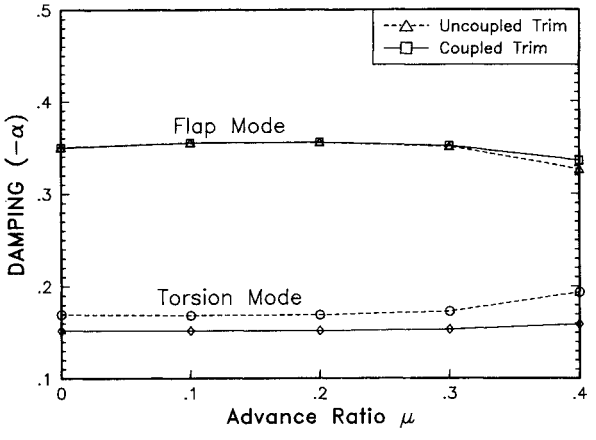

Fig. 2b Fundamental flap and torsion mode dampings.

Results and Discussion

A stability sensitivity analysis is carried out on a four-bladed hingeless rotor, Lock number $\gamma = 5.5$, solidity ratio $\sigma = 0.07$, thrust level $c_W/\sigma = 0.07$, blade aspect ratio $c/R = 0.055$, zero precone, and zero pretwist. The chordwise offsets of blade center of gravity, aerodynamic center, and tensile axis from the elastic axis (y_0, e_d, and e_A) are assumed to be zero for the baseline configuration. The fuselage c.g. lies on the shaft axis ($X_{CG} = Y_{CG} = 0$) and is located at a distance of $0.2R$ below the rotor hub center. The fuselage drag coefficient in terms of flat-plate area, i.e., $f/\pi R^2$, is taken as 0.01. The airfoil characteristics used are

$$c_\ell = 2\pi\alpha, \qquad c_d = 0.01, \qquad c_m = 0.0$$

For the baseline blade configuration (soft in-plane), the structural properties of the uniform blade are given in Table 1. These structural properties are chosen such that the desired rotating frequencies are obtained. The fundamental flap, lag, and torsional frequencies are 1.13/rev, 0.70/rev, and 4.47/rev, respectively. The numerical results are calculated for an advance ratio of 0.3, unless otherwise specified.

For the analysis, the blade is discretized into 5 beam elements of equal length, and each beam element consists of 15 nodal degrees of freedom. For the calculation of blade steady response, 8 coupled rotating natural modes (2 flap, 2 lag, 2 torsion, and 2 axial modes) are used. For the periodic response, one cycle of time is discretized into 6 time elements, and each time element is described by a quartic Lagrange polynomial distribution along the azimuth for motion. For the stability calculation, 2 flap, 2 lag, and 2 torsion modes are used because axial modes do not appear to have any important influence on blade stability. These modes are obtained about the mean deflected position of the blade. This modeling approximation yields satisfactory converged results.

Design parameters are considered nonstructural mass m_{ns}, chordwise offset of nonstructural mass y_{ns}, blade c.g. offset y_0, and blade flap bending stiffness (EI_y), lag bending stiffness (EI_z), and torsional stiffness (GJ). Design variables are selected among these design parameters. Furthermore, design variables have spanwise variations. Therefore, a total of 30 design variables for 5 beam elements are involved in the analysis.

For the coupled trim solution, couplings between the rotor and fuselage are included whereas, for the uncoupled trim solution, the rotor is isolated from the fuselage in the analysis. Figure 1 shows the blade steady flap response at the tip for an advance ratio of 0.3. The steady lag and torsional tip responses are found to have small differences between the two trim solutions. However, there is a considerable difference in the steady flap response. The result obtained by the coupled trim analysis shows primarily 2/rev flap response, whereas the result obtained using the uncoupled trim analysis shows a substantial 1/rev flap response. For a trimmed solution, there is no unbalanced force or moment acting on the hub. The lag and torsion responses consist primarily of 1/rev amplitudes, whereas the flap response is dominated by 2/rev amplitudes. Figure 2 presents the lag, flap, and torsion mode stability results for different advance ratios. Blade damping is represented in terms of the real part of the complex eigenvalue with a negative sign. It is also referred to as decay rate, which is a product of viscous damping and natural frequency. For the low damped lag mode stability, there is about an 8% reduction in the lag damping at $\mu = 0.3$ with the coupled trim solution. The flap mode damping shows comparatively less influence. For the torsion mode stability, a 13% increase in the torsion damping occurs at an advance ratio μ of 0.3 with the coupled trim solution. For $\mu \geq 0.3$, the influences become larger for all these modes.

To calculate sensitivity derivatives, two approaches are used: finite-difference and direct analytical approaches. For the finite difference, a central-difference scheme with 3% perturbations on either side of the baseline value is used. In Fig. 3, sensitivity derivatives of blade dampings obtained by finite-difference and analytical approaches are compared. These derivatives of blade damping with respect to design variables are evaluated at the midspan location. The numerical results obtained by these two approaches show identical trends.

Figure 4 shows CPU time on a UNISYS 1100/90 for the calculation of sensitivity derivatives of blade steady response, oscillatory hub loads, and blade dampings using finite-difference and direct analytical approaches. The CPU time required for the finite-difference approach increases linearly with re-

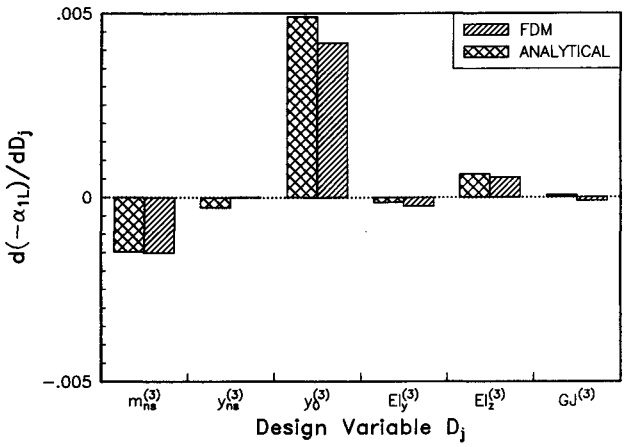

Fig. 3 Derivative of lag mode damping.

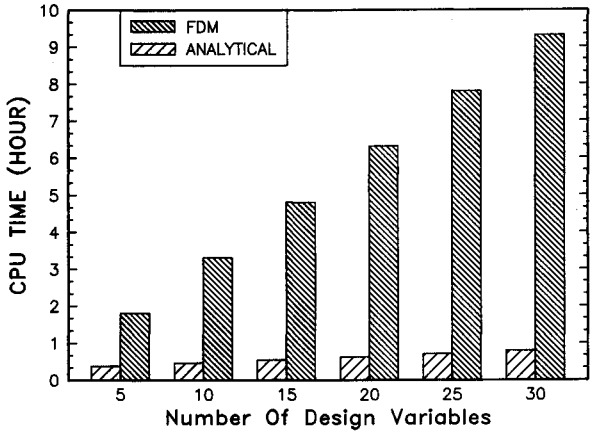

Fig. 4 CPU time for sensitivity analysis.

spect to a number of design variables, whereas it is barely increased by the use of the analytical method. For 30 design variables, there is about an 85% reduction in the CPU time when the direct analytical approach is used. The efficiency of this analytical approach indicates great potential for the rotor optimization problems.

To examine the sensitivity of blade damping to each design parameter, a systematic parametric study is presented. For nonstructural mass, there are two variables involved: nonstructural mass m_{ns} and its chordwise offset y_{ns}. For these parameters, centrifugal stiffening and inertial effects are involved. The Coriolis effect is also involved. These effects sometimes work against each other and hence make the interpretation of the results more difficult. Figure 5 shows the effects of nonstructural mass on stability of the lag, flap, and torsion modes. For this, a nonstructural mass of 5% blade weight is placed at various spanwise and chordwise locations. As expected, the effect of nonstructural mass becomes important for outboard elements. For the lag and flap modes, the addition of a nonstructural mass decreases damping, whereas the effect is small for the torsion mode. Adding a nonstructural mass not only increases the mass of the blade but also shifts the blade c.g. The chordwise blade c.g. offset from the elastic axis would result in coupling between the torsion and flap responses. In addition, the lag response is also coupled with these responses due to Coriolis effect. By suitable placement of a nonstructural mass, one can obtain favorable effects from these couplings. Placing a nonstructural mass at the 90% spanwise location shows a reduction in lag mode damping of 21% and in the flap mode damping of 19% from the baseline value. Placing a nonstructural mass at various chordwise locations has a negligible influence on the lag mode stability but has some influence on the flap mode stability. An aft location (say 35% chord) is more favorable than the forward location. For the 90% spanwise location, placing a nonstructural mass at the 35% chordwise position can increase the flap mode damping by 5% from the one obtained by placing it at the 15% chordwise position. For the torsion mode, the forward location of a nonstructural mass is generally favorable (see Fig. 5c). For example, near the blade tip (90% span), the placement of a nonstructural mass at the 15% chord location increases the torsion damping by 6% from the baseline value whereas, at the 35% chord location, it decreases damping by 18%. From these results, it is quite clear that the location of nonstructural mass, spanwise and chordwise, has some influence on blade stability.

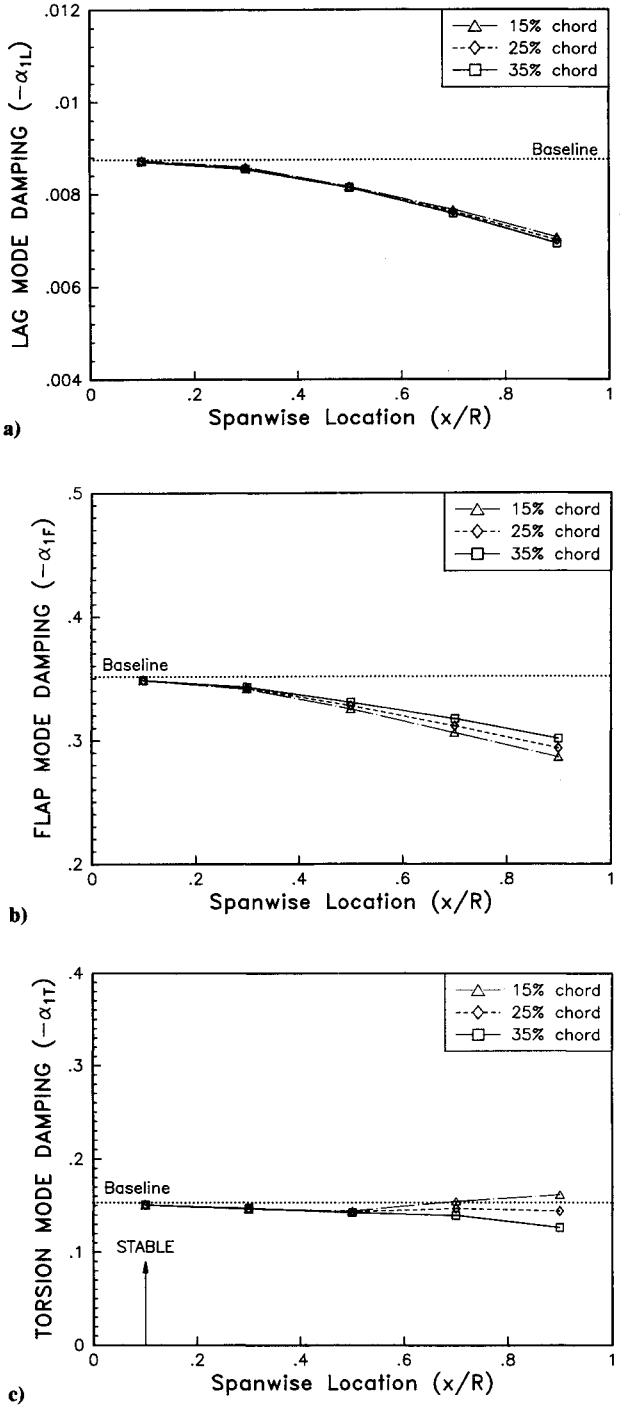

Fig. 5 Effect of nonstructural mass.

Figure 6 shows the effects of blade c.g. offset from the elastic axis on the lag, flap, and torsion modes stability. The elastic axis is assumed to coincide with the aerodynamic center (quarter-chord position). The chordwise blade c.g. offset is shifted forward (positive) or aft (negative) from the elastic axis, uniformly along the blade span. The mass is considered fixed as a baseline blade mass. The c.g. offset induces coupling between the torsion and flap responses. A forward shift of blade c.g. (ahead of quarter-chord) increases damping of the lag and torsion modes but reduces damping of the flap mode. With an aft location of the blade c.g., the opposite happens. For example, placing blade c.g. at the 35% chord location dampings of the lag and torsion modes are reduced by 11% and 88%, respectively, from the baseline values, whereas damping of the flap mode is increased by 32%. For the torsion mode, an aft position of the c.g. near the blade tip can result in static instability. From these results, it is clear that the blade c.g. offset has a powerful effect on blade stability.

Figure 7 shows the effects of blade bending stiffnesses on stability. For this, the bending stiffnesses are changed uniformly along the blade span. In reality, increasing stiffness is generally accompanied by an increase in rotor weight; however, for our calculations, weight is considered fixed. The variation in lag bending stiffness has an appreciable influence on the lag mode damping; with a 30% increase in lag bending stiffness, a 35% increase in the lag mode damping can be achieved. Lag mode damping is reduced with a decrease in lag bending stiffness and with an increase in flap bending and torsional stiffness. Flap mode damping is less sensitive to blade bending stiffness. Torsional mode damping is compara-

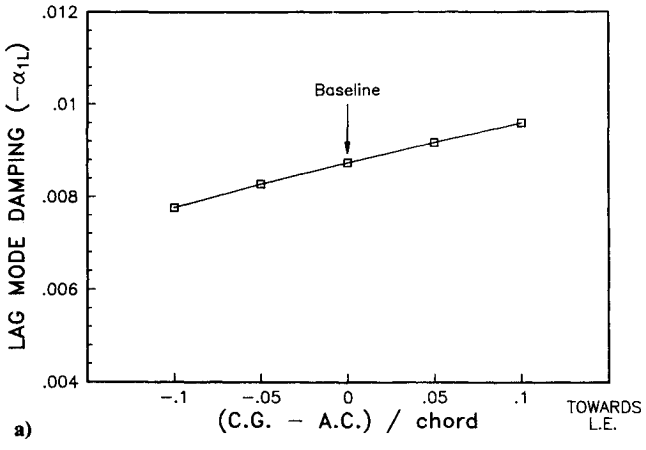

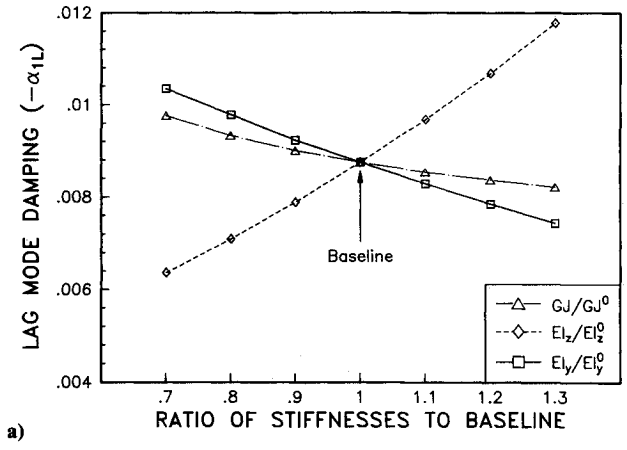

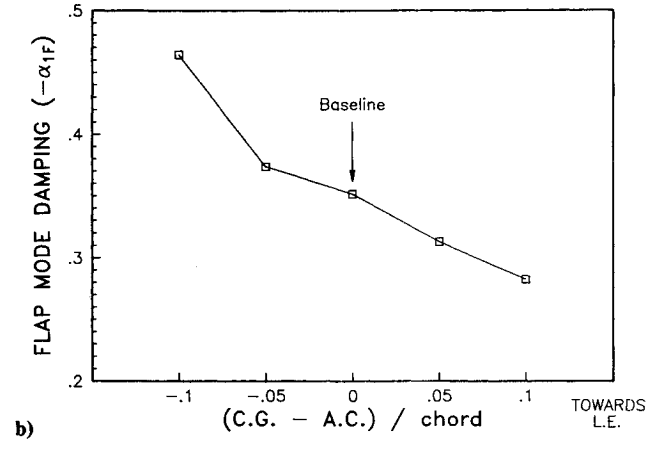

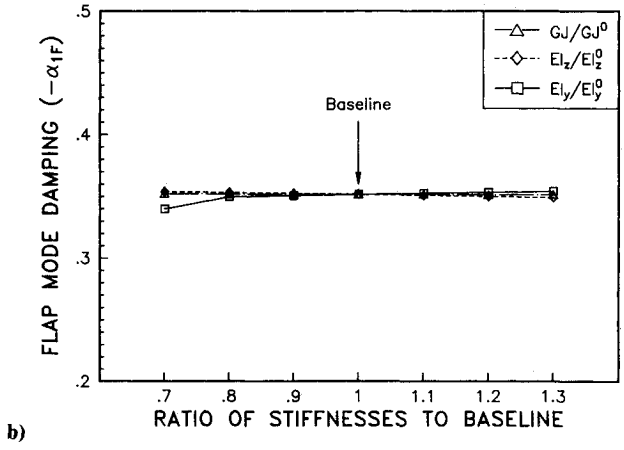

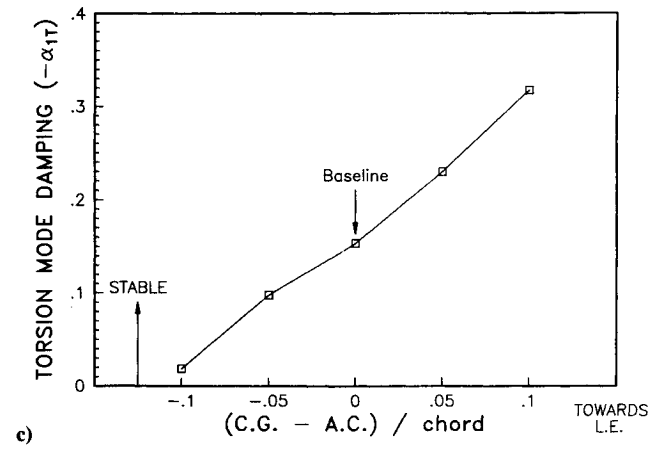

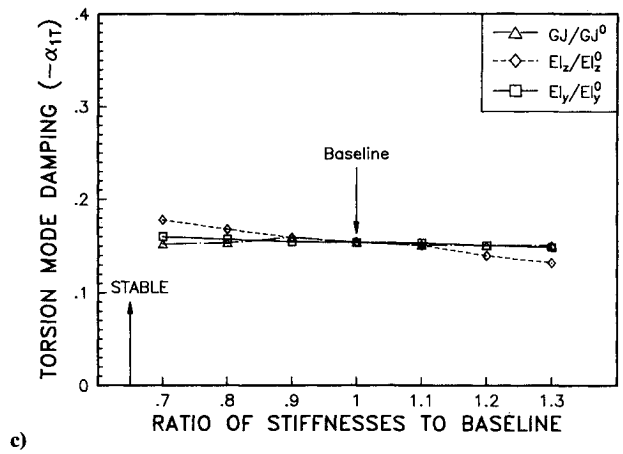

Fig. 6 Effect of blade center of gravity offset.

Fig. 7 Effect of blade bending stiffness.

tively less sensitive to flap bending and torsional stiffness than lag bending stiffness, however, and its influence is small.

In Fig. 8, the sensitivity derivatives of dampings with respect to design variables at different spanwise location are shown. By examining the magnitude of the derivatives, the sensitivity (local) to each design variable can be studied. For effective examination of the influence of nonstructural mass parameters, the sensitivity derivatives with respect to nonstructural mass and its chordwise offset are evaluated for a nonstructural mass of 5% blade mass uniformly distributed along the elastic axis. As expected, the influence of inertial parameters m_{ns}, y_{ns}, and y_0 on blade damping becomes larger for outboard elements (blade tip), whereas the influence of stiffness parameters EI_y, EI_z, and GJ on damping becomes generally larger for inboard elements (blade root). Lag mode damping is quite sensitive to nonstructural mass, blade c.g. offset, and lag bending stiffness; similar trends are observed in Figs. 5a, 6a, and 7a. For the flap mode, the largest influence on blade damping is due to the nonstructural mass and blade c.g. offset, and the influence of stiffness parameters is comparatively small; again, it confirms earlier observations made in Figs. 5b and 6b. For the torsion mode, the largest influence on the damping is due to the blade c.g. offset (refer to Fig. 6c), and the influence of nonstructural mass is comparatively small. The influence of lag bending and flap bending stiffness on the torsion mode damping becomes larger for the outboard elements, and the influence of torsional stiffness on the torsion damping is small.

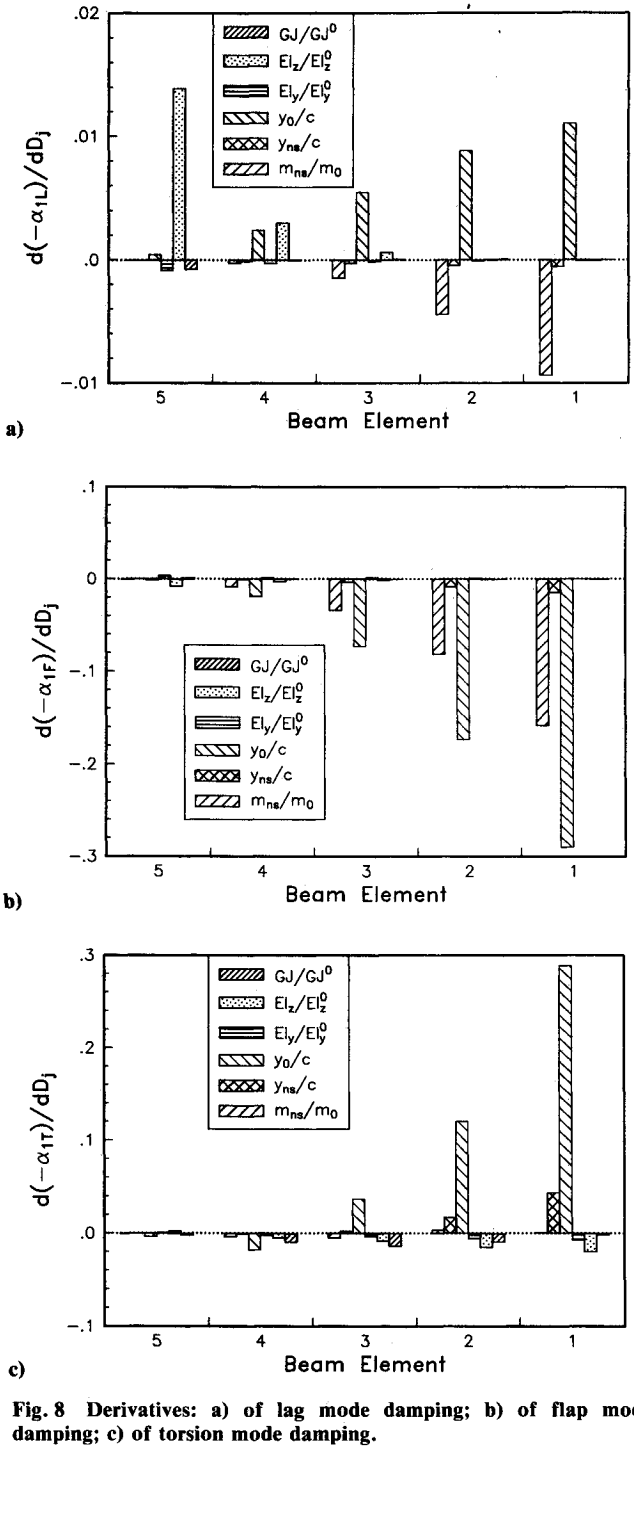

Fig. 8 Derivatives: a) of lag mode damping; b) of flap mode damping; c) of torsion mode damping.

Conclusions

Based on the results described here, the following conclusions are made:

1) A direct analytical approach is used successfully to calculate the stability sensitivity derivatives and shows a substantial reduction in CPU time compared to the finite-difference approach. (An 85% reduction in CPU time can be achieved by using a direct analytical approach.)

2) Lag mode damping is sensitive to nonstructural mass, blade c.g. offset, and lag bending stiffness; adding a nonstructural mass at outboard elements, an aft shift of the blade c.g. for outboard elements, and softening of lag bending stiffness for inboard elements decrease the lag damping considerably.

3) Flap mode damping is sensitive to nonstructural mass and blade c.g. offset; addition of a nonstructural mass at outboard elements and a forward shift of the blade c.g. for outboard elements decrease the flap damping considerably.

4) Torsion mode damping is sensitive to blade c.g. offset; an aft shift of the blade c.g. for outboard elements can result in static instability.

Acknowledgments

This work is supported by NASA Langley Research Center under NASA Grant NAG-1-739, technical monitor Joanne Walsh.

References

[1]Friedmann, P. P., "Application of Modern Structural Optimization to Vibration Reduction in Rotorcraft," *Vertica,* Vol. 9, 1985, pp. 363–373.

[2]Blackwell, R. H., "Blade Design for Reduced Helicopter Vibration," *Journal of the American Helicopter Society,* Vol. 28, July 1983, pp. 33–41.

[3]Taylor, R. B., "Helicopter Vibration Reduction by Rotor Blade Modal Shaping," *Proceedings of the 38th American Helicopter Society Annual Forum,* Anaheim, CA, May 1982.

[4]Friedmann, P. P., and Shanthakumaran, P., "Optimum Design of Rotor Blades for Vibration Reduction in Forward Flight," *Journal of the American Helicopter Society,* Vol. 29, April 1984, pp. 70–80.

[5]Peters, D. A., Rossow, M. P., Korn, A., and Ko, T., "Design of Helicopter Rotor Blades of Optimum Dynamic Characteristics," *Computation and Mathematics with Applications,* Vol. 12A, No. 1, 1986, pp. 85–109.

[6]Davis, M. W., and Weller, W. H., "Application of Design Optimization Techniques to Rotor Dynamics Problems," *Proceedings of the 42nd American Helicopter Society Annual Forum,* Washington, DC, June 1986, pp. 27–44.

[7]Bennett, R. L., "Application of Optimization Methods to Rotor Design Problems," *Vertica,* Vol. 7, 1983, pp. 201–208.

[8]Miura, H., "Applications of Numerical Optimization Methods to Helicopter Design Problems," *Vertica,* Vol. 9, 1985, pp. 141–154.

[9]Celi, R., and Friedmann, P. P., "Efficient Structural Optimization of Rotor Blades with Straight and Swept Tips," *13th European Rotorcraft Forum,* No. 3-1, Sept. 1987.

[10]Adelman, H. M., and Haftka, R. T., "Sensitivity Analysis of Discrete Structural Systems," *AIAA Journal,* Vol. 24, May 1986, pp. 823–832.

[11]Lim J. W., and Chopra, I., "Design Sensitivity Analysis for an Aeroelastic Optimization of a Helicopter Blades," *AIAA Journal,* Vol. 28, No. 1, Jan. 1990, pp. 75–82.

[12]Johnson, W., "Recent Development in the Dynamics of Advanced Rotor Systems," NASA TM-86669, March 1985.

[13]Friedmann, P. P., "Formulation and Solution of Rotary Wings Aeroelastic Stability and Response Problems," *Vertica,* Vol. 7, April 1983, pp. 101-141.

[14]Panda, B., and Chopra, I., "Dynamics of Composite Rotor Blades in Forward Flight," *Vertica,* Vol. 11, No. 1/2, 1987, pp. 187-209.

[15]Lim, J. W., and Chopra, I., "Aeroelastic Optimization of a Helicopter Rotor," *Journal of the American Helicopter Society,* Vol. 34, Jan. 1989, pp. 52-62.

[16]Friedmann, P. P., and Shamie, J., "Aeroelastic Stability of Trimmed Helicopter Blades in Forward Flight," *Vertica,* Vol. 1, No. 3, 1977, pp. 189-211.

[17]Panda, B., and Chopra, I., "Flap-Lag-Torsion Stability in Forward Flight," *Journal of the American Helicopter Society,* Vol. 30, April 1985, pp. 30-39.

[18]Lim, J. W., "Aeroelastic Optimization of a Helicopter Rotor," Ph.D. dissertation, Department of Aerospace Engineering, Univ. of Maryland, College Park, Maryland, May 1988.

[19]DeRusso, P. M., Roy, R. J., and Close, C. M., *State Variables for Engineers,* Wiley, New York, 1965.